Atmospheric
Chemistry
and Physics

The interplay between aqueous replacement reaction and the phase state of internally mixed organic/ammonium aerosols

Hui Yang, Fengfeng Dong, Li Xia, Qishen Huang, Shufeng Pang, and Yunhong Zhang

School of Chemistry and Chemical Engineering, Beijing Institute of Technology,
Beijing, 100081, People's Republic of China

Correspondence: Qishen Huang (qishenh@bit.edu.cn) and Shufeng Pang (sfpang@bit.edu.cn)

Abstract. Atmospheric secondary aerosols are often internally mixed with organic and inorganic components, particularly dicarboxylic acids, ammonium, sulfate, nitrate, and chloride. These complex compositions enable aqueous reaction between organic and inorganic species, significantly complicating aerosol phase behavior during aging and making phase predictions challenging. We investigated carboxylate–ammonium salt mixtures using attenuated total reflection Fourier-transformed infrared spectroscopy (ATR-FTIR). The mono-, di-, and tricarboxylates included sodium pyruvate (SP), sodium tartrate (ST), and sodium citrate (SC), while the ammonium salts included NH_4NO_3, NH_4Cl, and $(NH_4)_2SO_4$. Our results demonstrated that aqueous replacement reactions between carboxylates and ammonium salts were promoted by the formation and depletion of NH_3 as relative humidity (RH) changed. For SP/ammonium aerosols, $NaNO_3$ and Na_2SO_4 crystallized from 35.7 % to 12.7 % and from 65.7 % to 60.1 % RH, respectively, which is lower than the values for pure inorganics (62.5 ± 9 %–32 % RH for $NaNO_3$ and 82 ± 7 %–68 ± 5 % RH for Na_2SO_4). Upon hydration, the crystalline Na_2SO_4 and $NaNO_3$ deliquesced at 88.8 %–95.2 % and 76.5 ± 2 %–81.9 %, which is higher than the values of pure Na_2SO_4 (74 ± 4 %–98 % RH) and $NaNO_3$ (65 %–77.1 ± 3 % RH). In contrast, reaction between ST or SC and $(NH_4)_2SO_4$ was incomplete due to the gel structure at low RH. Unexpectedly, aqueous Na_2SO_4 crystallized upon humidification in ST/$(NH_4)_2SO_4$ particles at 43.6 % RH and then deliquesced with increasing RH. This is attributed to increased ion mobility in viscous particles, leading to nucleation and growth of Na_2SO_4 crystals. Our findings highlight the intricate interplay between chemical components within organic/inorganic aerosol and the impact of replacement reactions on aerosol aging, phase state, and subsequently atmospheric processes.

1 Introduction

The phase state of atmospheric aerosols is arguably one of the most crucial properties (Freedman et al., 2024), which dictates air quality, climate, and human health via processes including light absorption and scattering (Nemesure et al., 1995), cloud condensation nuclei (CCN) activity (Kreidenweis et al., 2005), chemical diffusion in aerosols, gas–particle partitioning (Shiraiwa et al., 2012), and heterogeneous reactions (Liu et al., 2016). However, the complex aerosol composition and various reaction pathways result in complicated aerosol phase behavior that is hard to predict

(Zhang et al., 2024). Understanding the phase behaviors and water content of atmospheric aerosols is therefore essential for elucidating their impacts on global climate and tropospheric chemistry.

Atmospheric aerosols are often composed of inorganic sulfates, nitrates, and organic species in varying mixing ratios (Riemer et al., 2019; Huang et al., 2014; Trebs et al., 2005; Zhou et al., 2019). The interaction between organic and inorganic components can alter the aerosol phase state and hygroscopicity (Shi et al., 2017; Wang et al., 2017; Marcolli and Krieger, 2006). Previous works have investigated the effect of organic acids on inorganic salts, showing the

impact of chemical composition and organic mass fractions (Huang et al., 2022; Jing et al., 2016). Recent field observations highlighted the significant role of organic acids in modifying the phase behavior of ammonium sulfate aerosols, further complicating the prediction of aerosol phase states (Li et al., 2021; Zhang et al., 2022; Kirpes et al., 2022). For atmospheric aerosols undergoing liquid–liquid phase separation (LLPS) with an organic shell and an inorganic core, black carbon redistribution can be induced, which leads to a more compact morphology and a reduction in the absorption enhancement effect by 28 %–34 % (Zhang et al. 2022). In addition, organic components can decrease aerosol surface activity (Petters and Kreidenweis, 2007) and drive the formation of viscous states at low humidity, leading to limited water absorption (Reid et al., 2018). Zhu et al. (2022) found that aqueous NaCl and $(NH_4)_2SO_4$ effloresced during humidification when they mixed with ultraviscous gluconic acid, showing high viscosity is another key regulator.

Aerosol phase state significantly influences chemical reaction within aerosols (Herrmann et al., 2015). Phase changes in aerosol components can enhance chemical reactions (Ma et al., 2022; Shao et al., 2018; Chen et al., 2021). For example, the photochemical HONO production from internally mixed $NaNO_3$-dicarboxylic acid aerosols is governed by the phase state of dicarboxylic acids (Li et al., 2024). In aqueous aerosols, the ions between two ionic compounds can exchange to form new compounds through aqueous replacement reactions. For instance, when oxalic acid mixes with nitrates, the H^+ ions can combine with NO_3^- ions to form HNO_3, which off-gases, leading to the formation of metal oxalate salts in the aerosol (Ma et al. 2019). Wang et al. (2019) first reported the aqueous replacement reaction between organic salts and ammonium sulfate to form organic acid, accompanying solid Na_2SO_4 formation. These reactions can generate gaseous compounds or less hygroscopic compounds, causing the substitution of weak bases for strong bases in aerosols (Yang et al., 2019; Du et al., 2020, 2021; Chen et al., 2022).

Despite the critical role of aerosol phase state, our understanding of the interplay between aerosol component reactivity, phase behavior, and water content remains limited. Reactions, such as replacement reaction, can alter aerosol phase state. The complexity of atmospheric aerosol phase states – including the coexistence of crystalline solid and liquid (Yang et al., 2019), liquid–liquid phase separation (Zhou et al., 2019), and solid in a viscous phase (Zhu et al., 2022) – can lead to inhomogeneity of aerosol components, which in turn affects their reactivity (Zong et al., 2022). The crystallization that accompanies these chemical reactions is a multi-step process involving ion migration, formation of ion pairs, nucleation, and growth processes. The extent of reaction, as well as the efflorescence relative humidity (ERH) and deliquescence relative humidity (DRH), can vary depending on the nature and molecular structure of the compounds involved. Therefore, investigating the interplay between differ-

ent organic and inorganic salts in terms of their reactivity and aerosol phase state is crucial for understanding atmospheric aerosols.

Organic acids are key components of atmospheric aerosols, each containing various functional groups with distinct physicochemical properties. Similarly, sulfates, chlorides, and nitrates exhibit unique characteristics. To investigate the impact of organic salts on phase behavior and chemical reactions, we mixed sodium tartrate, sodium citrate, and sodium pyruvate – representing mono-, di-, and tricarboxylates – with ammonium sulfate. We also examined the effects of inorganic ions by mixing ammonium nitrate with sodium pyruvate. Molar ratios of 1 : 2, 1 : 1, and 2 : 1 were used to simulate surplus organic salts, an equal amount of organic salts, and excessive inorganic salts in mixed sodium pyruvate and ammonium chloride aerosols, reflecting variations by location, aerosol source, and season. Attenuated total reflection Fourier-transform infrared spectroscopy (ATR-FTIR) was employed to monitor changes in phase and composition during chemical reactions. This study improves our understanding of the interplay between aerosol composition, replacement reactions, and phase states in organic–inorganic aerosols, which is crucial for better predicting aerosol phase states and assessing their effects on climate.
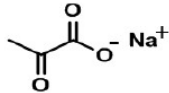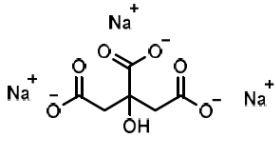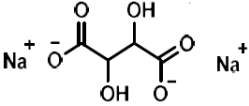
2 Materials and methods

2.1 Sample preparation

The $0.2\,mol\,L^{-1}$ mixture solutions of organic acid salts and ammonium salts were prepared using triple-distilled water. The organic acid salts include sodium pyruvate (SP; Aladdin Reagent Co., Ltd., $\geq 99.0\,\%$), sodium citrate (SC; Beijing Chemical Reagents Company, $\geq 99.0\,\%$), and sodium tartrate (ST; Beijing Chemical Reagents Company, $\geq 99.0\,\%$). The ammonium salts include $(NH_4)_2SO_4$, NH_4NO_3, and NH_4Cl (all from Beijing Chemical Reagents Company, $\geq 99.0\,\%$). In a mixture system, one organic acid salt was mixed with one type of ammonium salt at various molar ratios (e.g., 2 : 1, 1 : 1, 2 : 3, and 1 : 2). In the atmosphere, the organic to inorganic ratio varies regionally but mostly remains at the same order of magnitude. Thus, the selected ratios herein can effectively represent different regions. The mixture solutions were aerosolized into aerosol droplets with an average diameter of $5\,\mu m$. All compounds were used without further purification before the experiment. The molecular structure and properties of the compounds involved in this study are listed in Table 1.

2.2 ATR-FTIR measurement

The ATR-FTIR measurement was conducted using a FTIR spectrometer (Nicolet Magna IR 560 model) equipped with a liquid-nitrogen-cooled mercury–cadmium–telluride (MCT) detector. An RH-controlling system, composed of a high-

Table 1. The molecular structure of inorganic and organic compounds.

Compound	Molecular structure	Dissociation constant of conjugate acid	Solubility in 100 g H_2O (20 °C)	Molecular weight (Da)
Ammonium nitrate	NH_4NO_3	NA	190 g	80.043
Ammonium chloride	NH_4Cl	NA	37.2 g	53.49
Ammonium sulfate	$(NH_4)_2SO_4$	NA	75.4 g	132.14
Sodium pyruvate		$K_a = 3.2 \times 10^{-3}$	47 g	82.03
Sodium citrate		$K_{a,1} = 7.4 \times 10^{-4}$ $K_{a,2} = 1.7 \times 10^{-5}$ $K_{a,3} = 4.0 \times 10^{-7}$	154 g	258.07
Sodium tartrate		$K_{a,1} = 1.04 \times 10^{-3}$ $K_{a,2} = 4.55 \times 10^{-5}$	33.3 g	194.05

NA: not available.

purity water reservoir, mass flowmeter, and vacuum pump, was connected to the FTIR spectrometer. The RH was controlled by the mixing ratio of a wet nitrogen gas flow (saturated by water vapor) and a dry nitrogen gas flow. The total flow rate of the two nitrogen gas flows was 500 mL min^{-1}, and the flow rates of the wet and dry nitrogen gas flows were controlled by mass flow controllers. During the experiments, the RH was monitored by humidity with a precision of 0.5 % and an accuracy of 1 % and temperature sensors coupled to a data logger at the outlet of the sample chamber. Detailed instrumental information can be found in Zhang et al. (2014). Prior to the ATR-FTIR measurement, the RH was kept at the highest level in the sample chamber. The aerosols were atomized and introduced into the sample chamber to be deposited onto the ZnSe substrate under the high-RH condition. At room temperature, the spectral resolution and the spectral range of the ATR-FTIR are 4 cm^{-1} and 800–4000 cm^{-1}, respectively.

2.3 Data processing

The IR spectra of aerosols were obtained by subtracting the IR spectra of water vapor at corresponding RH from raw IR spectra without any smoothing. The water content at each RH level was gained by integrating the bands at 3360–3690 cm^{-1} in the corresponding IR spectra. The relative water content was achieved by normalizing the peak area of the water band

(3360–3690 cm^{-1}) at a specific RH to that at the maximum RH.

3 Results and discussion

The phase behavior of mixed aerosols is dependent upon the chemical composition, molar ratio, and chemical process. Herein we selected three organic salts, including SP, ST, and SC, along with NH_4Cl, NH_4NO_3, and $(NH_4)_2SO_4$, to study the interplay between phase state, composition evolution, and aqueous-phase replacement reactions in aerosols during RH changing cycles. This section consists of seven parts. In Sect. 3.1, we analyze the IR spectra of pure organic salts and inorganic salts to obtain the differences in characteristic peaks for aqueous and solid phases. Based on this, in Sect. 3.2, SP is mixed with different ammonium salts with various stoichiometric ratios to form aerosols, and the infrared spectra of the mixed aerosols are tested to analyze the characteristic absorption peaks in the second section. The results showed that SP underwent a substitution reaction with the ammonium salts, and the mixed aerosols containing different ammonium salts exhibited distinct phase behaviors. Therefore, in Sect. 3.3 and 3.4, we discuss in detail the substitution reactions and the resulting changes in water content and phase transition regions of the compounds. The phase transition regions of the reaction products are compared with those of the pure components. The relative content of the

mixed components may vary in different regions. In Sect. 3.5, we take the SP/NH$_4$Cl system as an example to study the impact of different component contents on phase transition behavior. After investigating the hygroscopic behavior of mixed aerosols containing different ammonium salts with the same organic salt, in Sect. 3.6, we examine the phase evolution of aerosols induced by mixing different organic salts, SC and ST, with ammonium sulfate. By combining infrared spectroscopy and optical images, we discovered that the mixture of tartaric acid and ammonium sulfate not only underwent substitution reactions but also exhibited unexpected hygroscopic weathering behavior. Therefore, in Sect. 3.7, we discuss the causes of this special phase behavior.

3.1 Spectral change in and phase behavior of pure inorganic and organic aerosols

The IR spectra of individual components, namely ammonium nitrate, ammonium sulfate, ammonium chloride, sodium pyruvate, sodium citrate, and sodium tartrate, are shown in the supporting information (Fig. S1 in the Supplement), and band assignments can be found in Table S1 in the Supplement. The features of the IR spectra can be used to differentiate between the phase state of each compound. For example, for sodium tartrate, the characteristic peaks of the aqueous phase and crystalline solid phase are located at 1069 and 1055 cm^{-1}, respectively. Sodium citrate exhibits double sharp peaks at 1308 and 1278 cm^{-1} during crystallization. For pure sodium pyruvate, the characteristic peaks of solid phase appear at 1405 cm^{-1}, and the band at 1176 cm^{-1} is shifted to 1186 cm^{-1}. As for crystalline solid NH$_4$Cl, bands at 3130 and 1402 cm^{-1} are the characteristic IR peaks. When NH$_4$Cl is mixed with sodium pyruvate, the band at 1402 cm^{-1} may overlap with 1405 cm^{-1} and become indistinguishable; therefore, the band at 3130 cm^{-1} was used as the feature for crystalline solid NH$_4$Cl, and the band at 1186 cm^{-1} was applied to characterize crystalline solid sodium pyruvate. For NH$_4$NO$_3$ and (NH$_4$)$_2$SO$_4$, when the phase transition from aqueous to crystalline solid phase occurs, the NH$_4^+$ bands exhibit dissimilarity: shifting from 1448 to 1417 cm^{-1} for NH$_4$NO$_3$ and from 1443 to 1412 cm^{-1} for (NH$_4$)$_2$SO$_4$. When NH$_4$NO$_3$ and (NH$_4$)$_2$SO$_4$ are mixed with organic salts, the NH$_4^+$ bands can overlap with the characteristic peaks of sodium citrate and sodium tartrate in the same wavenumber region, leading to difficulties in assigning the peaks to specific crystalline solid ammonium salts.

The IR spectra on dehydration and hygroscopic behavior of organics (sodium pyruvate, sodium citrate, and sodium tartrate) during RH change are shown in Fig. 1. For pure organic compounds, the response of water content in aerosols can be applied to elucidate phase transition. Sodium pyruvate aerosols effloresced at 63 %–60.5 % RH upon dehydration, corresponding to a sudden change in water content. In comparison, the water content of pure sodium citrate and sodium tartrate aerosols decreased gradually upon dehumid-

ification, retaining normal water content values of 0.25 and 0.15 for ST and SC, respectively, at the lowest RH, indicating the formation of a viscous state instead of crystalline solid phase (Mikhailov et al., 2009). The formation of a viscous phase was also consistent with the absence of crystalline solid features in IR spectra and the residual water peak at 3360 cm^{-1}. Upon humidification, sudden water uptake occurred at 47.1 %–49.8 % RH for sodium citrate and at 55.7 %–59 % RH for sodium tartrate aerosols, where the error margin is 1 %. A previous study has shown that similar abrupt water absorbance during humidification was observed for viscous sucrose (Madawala et al., 2021) and MgSO$_4$ aerosols (Wang et al., 2018), which was attributed to the hydration of aerosols during the phase transition from a gel state to an aqueous state. Hence, the abrupt change in water content of the sodium citrate and sodium tartrate aerosols is due to the phase transition from a viscous state to an aqueous state.

3.2 Spectral change in and phase behavior of mixed organic/inorganic aerosols

Sodium pyruvate (SP) was mixed with various ammonium salts, including (NH$_4$)$_2$SO$_4$, NH$_4$Cl, and NH$_4$NO$_3$, as a molar ratio of 2 : 1, 1 : 1, and 1 : 2, respectively. Figure 2 illustrates their IR spectra as the RH decreased. The data for SP/(NH$_4$)$_2$SO$_4$ (Fig. 2a) have been reported by Yang et al. (2019). The band at 3400 cm^{-1}, assigned to the OH stretching mode of water, became weaker upon dehydration, suggesting a gradual loss of liquid water content. Concurrently, the bands at 1708 and 1355 cm^{-1} gradually diminished, indicating a decrease in the quantity of SP in the aerosol phase. In the blue frame of Fig. 2a, the enlarged IR feature of SP depicts the gradual weakening of the 1176 cm^{-1} peak, which disappeared at 65.7 % RH, implying complete SP depletion from the aerosols. The overlapping nature of the v_4-NH$_4^+$ mode, located at ~ 1440 cm^{-1} in the aqueous phase or 1412 cm^{-1} in the crystalline solid phase, with the bands of SP at 1424 or 1406 cm^{-1}, renders the determination of the phase state of (NH$_4$)$_2$SO$_4$ ambiguous. Accompanying the SP depletion, we noted the appearance of a band at 1132 cm^{-1} at 65.7 %, followed by its subsequent increase with further decreasing RH. Tan et al. (2014) investigated the efflorescence of Na$_2$SO$_4$ and assigned the 1132 cm^{-1} band to crystalline solid Na$_2$SO$_4$. In addition, the v_1-SO$_4^{2-}$ mode effectively discerns the sulfate phase state, with a peak at 980 cm^{-1} indicating the aqueous state and a peak at 996 cm^{-1} denoting the crystalline solid state (Miñambres et al., 2013). The purple frame in Fig. 2a shows the emergence of the 995 cm^{-1} band at 65.5 % RH, accompanied by the diminishing 980 cm^{-1} band. At 60.1 % RH, the 980 cm^{-1} disappeared, indicating the complete crystallization of Na$_2$SO$_4$.

For SP/NH$_4$Cl aerosols, the IR bands for SP at 1708, 1355, and 1627 cm^{-1} became weaker at lower RH levels (Fig. 1b), indicating the decrease in SP content. As depicted in the
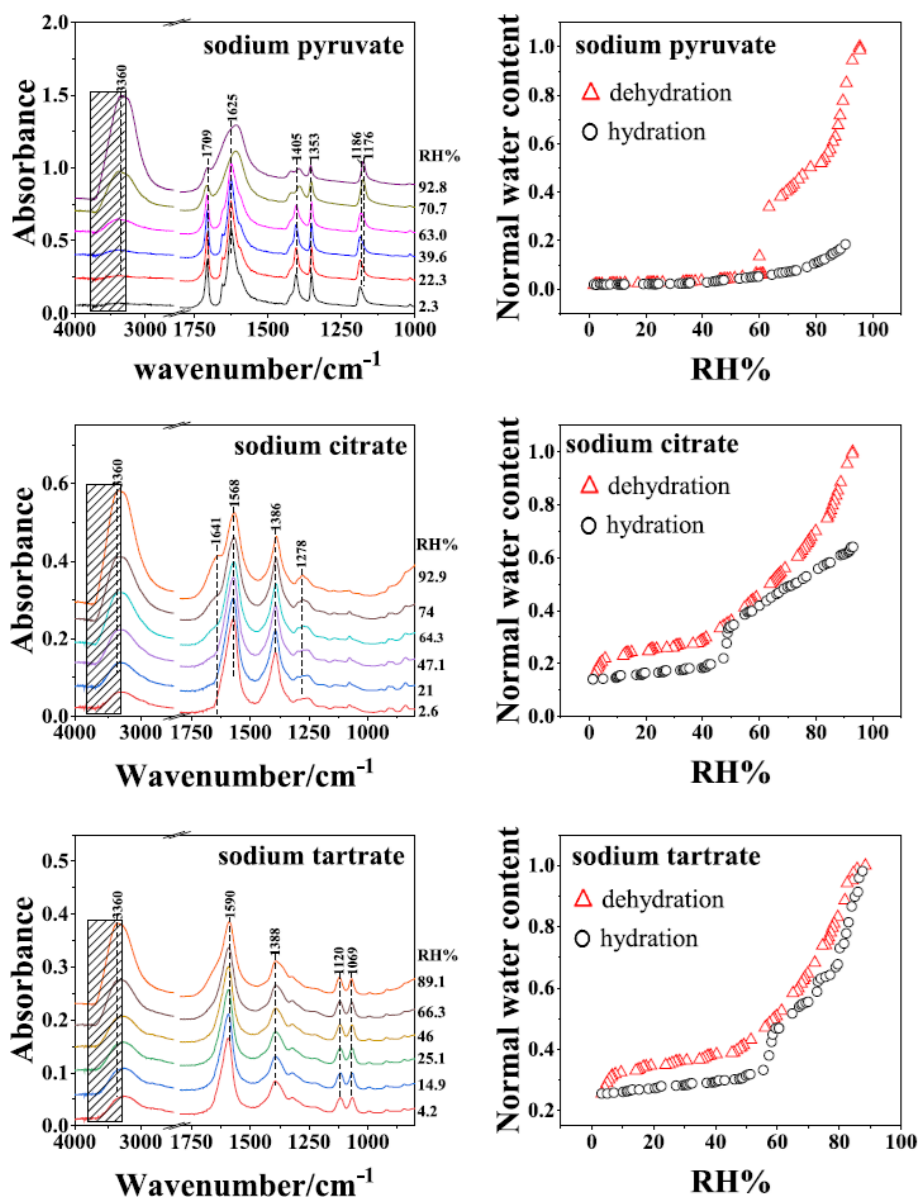
Figure 1. The IR spectra of organic salts with respect to dehydration and hygroscopic behavior during a down-up RH cycle. Boxes with diagonal hatching show the chosen integration region for liquid water. The spectra for sodium pyruvate have previously been reported by Yang et al. (2019).

blue frame in Fig. 2b, both the crystalline solid IR band ($1186 \, cm^{-1}$) and the aqueous IR band of SP ($1176 \, cm^{-1}$) can be found at and below 23.7 % RH, implying the co-existence of liquid and crystalline solid SP in SP/NH$_4$Cl aerosols. Additionally, the band at $1404 \, cm^{-1}$ became prominent at 42.5 % RH. Given the comparable peak height between 1353 and $1405 \, cm^{-1}$ in the IR spectrum of crystalline solid SP, the band at $1404 \, cm^{-1}$ likely originated from crystalline solid NH$_4$Cl, consistent with the sharp bands at 3130 and $3036 \, cm^{-1}$ (Max and Chapados, 2013). According to previous studies, NaCl should form in the system; however,

the formation of NaCl cannot be confirmed merely from the IR spectrum as NaCl exhibits no IR absorptions.

For SP/NH$_4$NO$_3$ particles, we observed similar SP loss, denoted by weaker SP band adsorption upon dehydration, along with a stronger band at $1355 \, cm^{-1}$, an IR feature corresponding to the efflorescence of NaNO$_3$ (1352 and $836 \, cm^{-1}$) (Ren et al., 2016). When RH decreased to 35.7 %, the band for crystalline solid NaNO$_3$ at $836 \, cm^{-1}$ appeared (Fig. 2c, purple frame), coexisting with the $829 \, cm^{-1}$ band for aqueous NO$_3^-$, indicating the presence of liquid NO$_3^-$ across the RH range of 35.7 %–32 %. At 12.7 % RH, only the band at $836 \, cm^{-1}$ was present, suggesting the crystal-
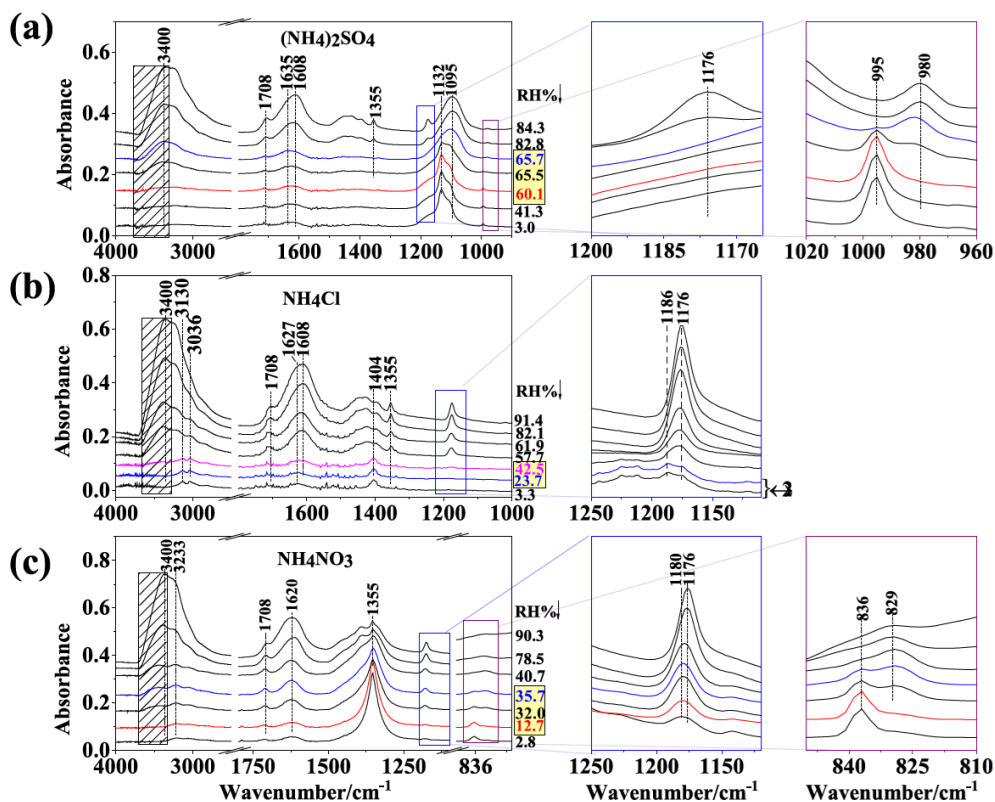
Figure 2. The FTIR spectra of mixed aerosols containing sodium pyruvate and various ammonium salts measured in this study and in previous work. **(a)** Ammonium sulfate (Yang et al., 2019), **(b)** ammonium chloride, **(c)** ammonium nitrate on dehydration. The spectral data for sodium pyruvate and ammonium sulfate have previously been reported by Yang et al. (2019). Boxes with diagonal hatching show the chosen integration region for liquid water. The yellow frame indicates the RH range when phase transition occurs (ERH of Na_2SO_4: 67.5 %–60.1 %; onsets of ERH for SP and NH_4Cl: 23.7 % and 42.5 %; ERH of $NaNO_3$: 35.7 %–12.7 %).
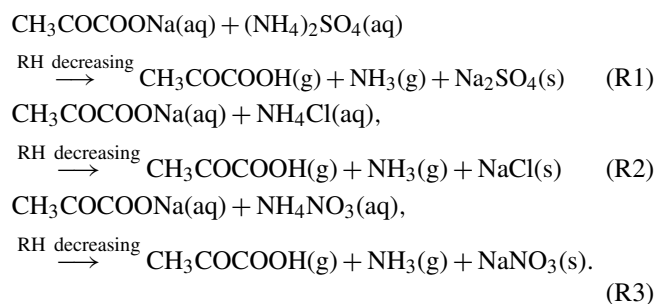
lized $NaNO_3$ without liquid NO_3^- (Zhang et al., 2014). In the blue frame of Fig. 2c, the band at $1176\,cm^{-1}$ shifts slightly to $1180\,cm^{-1}$ instead of the crystalline solid SP band at $1186\,cm^{-1}$, suggesting semi-solid SP rather than crystalline solid SP.

Following the dehydration, the hydration of three SP/ammonium aerosols was performed. Figure S2 in the Supplement presents the IR spectra on hydration. As the RH increased, the water content of the three SP/ammonium mixture systems increased, characterized by the bands at $3355/3400$ and $1640\,cm^{-1}$ as seen from Fig. S2. The characteristic bands of SP became negligible, indicating trace or no SP remaining in aerosols, while for SP/$(NH_4)_2SO_4$ aerosols, only the $995\,cm^{-1}$ band was found below 88.8 % RH, indicating crystalline solid Na_2SO_4 without liquid SO_4^{2-} in the particles. From 88.8 % RH, two bands are present at 980 and $995\,cm^{-1}$, indicating the coexistence of liquid SO_4^{2-} and crystalline solid Na_2SO_4. As the RH continues to rise, the $995\,cm^{-1}$ band decreased rapidly and then almost vanished at 95.2 % RH, suggesting the deliquescence of aerosols. In the IR spectra of SP/NH_4Cl aerosols, the bands from crystalline solid NH_4^+, i.e., 3130, 3036, and $1404\,cm^{-1}$, de-

creased gradually and disappeared at 71.8 % RH, indicating the depletion of ammonium during hydration. In the IR spectra of SP/NH_4NO_3 particles, the band at $829\,cm^{-1}$ begins to appear at 76.5 %, indicating the dissolution of solid $NaNO_3$. When the RH reached 81.9 %, the band at $836\,cm^{-1}$ disappeared, suggesting complete deliquescence of $NaNO_3$.

3.3 The replacement reactions in SP/ammonium aerosols and the resulting hygroscopicity

The above analysis on IR features showed Reactions (R1)–(R3) in mixed SP/ammonium aerosols:

$$CH_3COCOONa(aq) + (NH_4)_2SO_4(aq)$$

$$\xrightarrow{RH\ decreasing} CH_3COCOOH(g) + NH_3(g) + Na_2SO_4(s) \quad (R1)$$

$$CH_3COCOONa(aq) + NH_4Cl(aq),$$

$$\xrightarrow{RH\ decreasing} CH_3COCOOH(g) + NH_3(g) + NaCl(s) \quad (R2)$$

$$CH_3COCOONa(aq) + NH_4NO_3(aq),$$

$$\xrightarrow{RH\ decreasing} CH_3COCOOH(g) + NH_3(g) + NaNO_3(s). \quad (R3)$$

It can be seen that pyruvic acid and ammonia are formed and depleted from particles alongside the crystalline solid formation of various inorganic salts during dehydration, which proceeded the replacement reaction between SP and ammonium. Herein, aerosol particles act as micro-reactors, with their larger specific surface area compared to bulk solution facilitating similar processes. In fact, the replacement reactions in aerosols driven by released gas or compound formation with lower solubility have been reported in previous work. For example, Wang et al. (2017) observed the reaction in aerosols composed of oxalic acid and ammonium sulfate, which was driven by formation of lower-hygroscopic ammonium hydrogen oxalate ($NH_4HC_2O_4$) and ammonium hydrogen sulfate (NH_4HSO_4) during the dehydration process, and Wang et al. (2019) addressed the formation of crystalline solid Na_2SO_4 from $(CH_2)_n(COONa)_2$ ($n = 1, 2$)/$(NH_4)_2SO_4$ aerosols upon dehydration. Building upon their findings, crystalline solid $NaNO_3$ and $NaCl$ are also formed, as shown in Reactions (R2) and (R3).

The phase state of aerosol particles strongly depends on their water content, which in turn is influenced by changes in ambient RH (Yeung and Chan, 2010). Conventionally, soluble inorganic aerosol particles spontaneously absorb water to form solution droplets upon hydration, and these droplets recrystallize upon dehydration. Pure inorganic particles, such as $NaCl$ and $(NH_4)_2SO_4$, often undergo prompt phase transitions reflected by sudden water loss or uptake (Martin, 2000). Conversely, pure organic aerosols exhibit more diverse hygroscopic behaviors, forming either (poly)crystalline states or semi-solids (Kuang et al., 2010). When mixtures of compounds are present in aerosols, as is ubiquitous in atmospheric aerosols and in $PM_{2.5}$, phase transitions may occur for all components or only a portion of them. Even if all constituents effloresce, the critical RH values vary compared to pure compounds. Consequently, the water content may not be indicative of the efflorescence or deliquescence process. For aerosols composed of sodium pyruvate and ammonium, the response of water content to ambient RH is dependent upon the water vapor equilibrium, replacement reaction, product depletion, and phase transitions. Therefore, changes in water content and IR spectra of aerosols need to be considered collaboratively to accurately understand the reactions and phase transitions of these aerosols.

Figure 3 shows the water content evolution during an RH cycle and its comparison with the phase transition points of compounds. The RH changes stepwise, and the rate is $< 5\% \, min^{-1}$. The stay time at each level is 30 min to allow for equilibration between particles and the surrounding RH. A significant deviation between the RH at which phase changes occur and the RH at which water content changes abruptly can be observed. We note that the SP/$(NH_4)_2SO_4$ data have previously been reported in Yang et al. (2019). The sensitive RH range for SP/$(NH_4)_2SO_4$, where abrupt water loss occurs, ranged from $66.5 \pm 1\%$ to $59.8 \pm 1\%$ RH,

overlapping with the phase change RH of Na_2SO_4 shown by the red frame during dehydration in Fig. 3a. Conversely, the deliquescence range of Na_2SO_4 (pink frame) occurs at higher RH values than the abrupt water absorption range of $74.4 \pm 1\%$ to $87.3 \pm 1\%$ RH during hydration in Fig. 3a. In the case of SP/NH_4Cl, the coexistence of aqueous and crystalline solid SP (red frame) occurs at RH values that are much lower than the range of sudden water loss ($61.7 \pm 1\%$ to $42.2 \pm 1\%$ RH) in Fig. 3b. When the RH increases, obvious water uptake takes place from $68.9 \pm 1\%$ RH to $80.9 \pm 1\%$ RH. In previous studies, NH_4NO_3 was often believed to form a viscous gel, leading to gradual dehydration with decreasing RH (Y. J. Li et al., 2017). However, the produced $NaNO_3$ undergoes an aqueous-to-solid transformation within the RH range of $35.7 \pm 1\%$ to $12.7\% \pm 1\%$, shown in the red frame in Fig. 3c, while maintaining an almost constant water content. During hydration, excessive water absorption occurs in the range of $72.7\% \pm 1\%$ to $82.1 \pm 1\%\%$ RH, covering the deliquescence RH of $NaNO_3$ (pink frame in Fig. 3c).

3.4 The effect of organics on phase transition point

When inorganic compounds are mixed with organics, the efflorescence and deliquescence points are modified due to intermolecular interactions. For instance, organic acids have been found to influence the phase transitions and water uptake of ammonium sulfate (AS) aerosols (Shi et al., 2017). Similarly, organic salts can enhance water uptake, sometimes reaching levels comparable to those of typical inorganic salts such as $NaCl$ and $(NH_4)_2SO_4$. Wu et al. (2011) observed a clear shift in the deliquescence relative humidity (DRH) of AS towards lower RH values for mixtures of AS with organic acid salts, resulting in enhanced water uptake relative to mixtures with organic acids alone. Additionally, Schroeder and Beyer (2016) noted that the onset DRH of organic salt–AS mixtures was consistently lower than that of the pure components, irrespective of the fraction of organic salts in the mixture.

Figure 4 illustrates the RH ranges of efflorescence and deliquescence for comparison. It demonstrates the lower efflorescence relative humidity (ERH) of Na_2SO_4, $NaNO_3$, and SP in mixtures compared to those in pure aerosols, indicating that the presence of organics in the mixed particles can inhibit the crystallization of the produced inorganics. In contrast to crystallization, the DRHs of Na_2SO_4 and $NaNO_3$ in mixtures were slightly higher than those of pure aerosols with a narrower DRH range. This deviates from previous experimental measurements and thermodynamic model predictions, which have suggested a significant reduction in aerosol DRH due to the mixing of organic acids and inorganic salts (Bouzidi et al., 2020; Hodas et al., 2015).
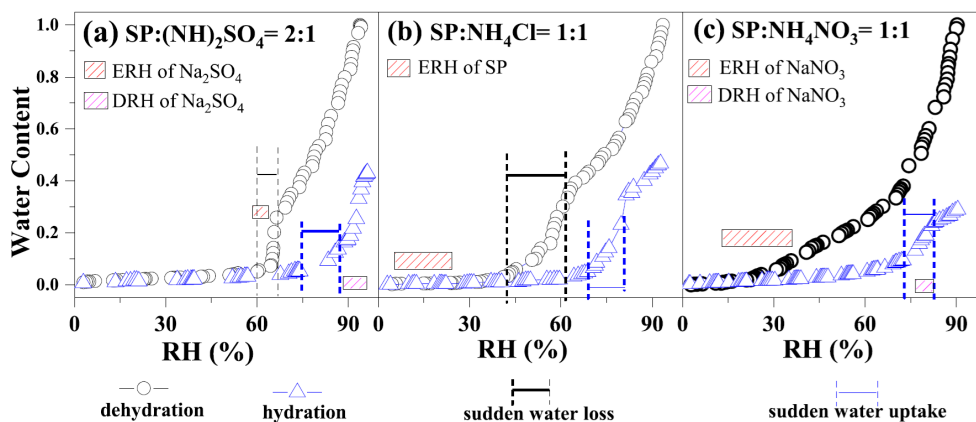
Figure 3. Hygroscopicity curve of (a) SP: $(NH_4)_2SO_4 = 2:1$ aerosols, (b) SP: $NH_4Cl = 1:1$ aerosols, and (c) SP: $NH_4NO_3 = 1:1$ aerosols. The data for aerosols with SP: $(NH_4)_2SO_4 = 2:1$ have previously been reported by Yang et al. (2019). The stoichiometric ratio between SP and $(NH_4)_2SO_4$ was set to $2:1$ to keep an equivalent amount of organics and ammonium. In comparison, SP/NH_4Cl aerosols and SP/NH_4NO_3 aerosols also have an equivalent amount of organics and ammonium.
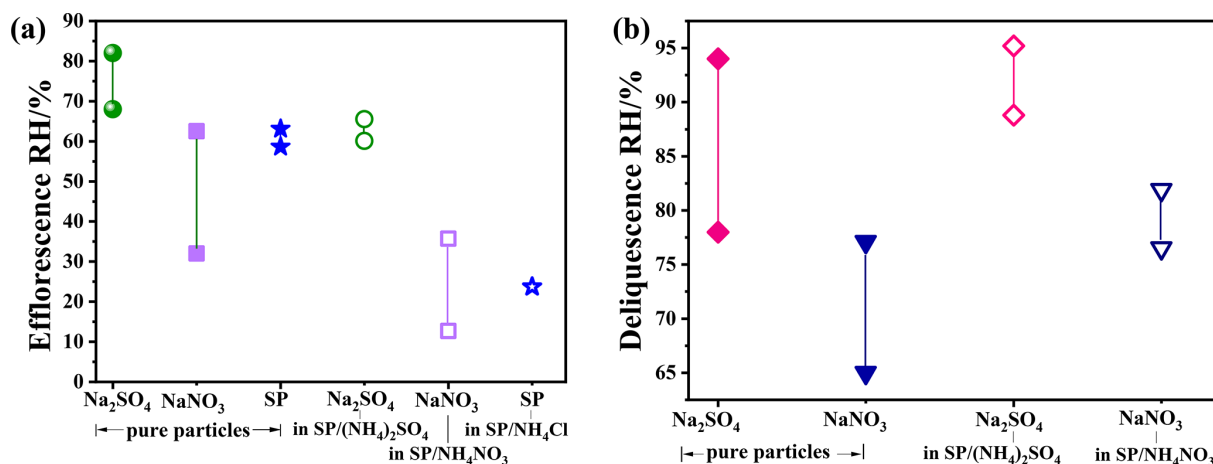

Figure 4. The efflorescence RH (a) and deliquescence RH (b) for single-component aerosols (pure particles) and SP/ammonium particles.

3.5 The effect of molar ratio on the replacement reaction and phase transition

The chemical reactivity and phase state of aerosols are often influenced by individual compounds within internally mixed particles. In this study, SP/NH_4Cl particles were selected as a surrogate to investigate the dependence of component reconstruction and phase transition on the molar ratio of SP to NH_4Cl. A mixture of SP/NH_4Cl aerosols were prepared with molar ratios of $1:2$, $1:1$, and $2:1$. Figure S3 in the Supplement presents the IR spectra in the range of 4000–$800\,cm^{-1}$ for $2:1$, $1:1$, and $1:2$ SP/NH_4Cl ratios. When the molar ratio of SP to NH_4Cl was $2:1$, the band changes were reversible during the dehydration and hydration cycle, with the absence of the $3130\,cm^{-1}$ $\nu(NH_4^+)$ band of solid NH_4Cl. The band shift between 1608 and $1627\,cm^{-1}$ indicated the transition of SP between the liquid and crystalline solid phases.

For $1:1$ SP/NH_4Cl particles, the IR spectra are shown in Figs. 2b and S2b and are described above. In the case of $1:2$ SP/NH_4Cl aerosols, the band at $3130\,cm^{-1}$ was observed at $46.6\,\%$ RH during dehumidification and disappeared at $77.7\,\%$ RH during humidification. Following a dehumidification–humidification cycle, the overall quantity of compounds within the aerosol particles decreased, as reflected by the lower IR band intensity.

Figure S4 in the Supplement displays the IR spectra in the range of 1220–$1120\,cm^{-1}$ during dehydration, providing detailed band shift and intensity information of the $1176\,cm^{-1}$ band. Additionally, the quantified peak position and integrated peak areas of SP/NH_4Cl particles, which can characterize the phase state and degree of chemical reaction, are depicted in Fig. 5. The band at $1176\,cm^{-1}$ indicates that the aerosols are in the aqueous phase, while its shift to $1186\,cm^{-1}$ signifies the transition to crystalline solid-phase
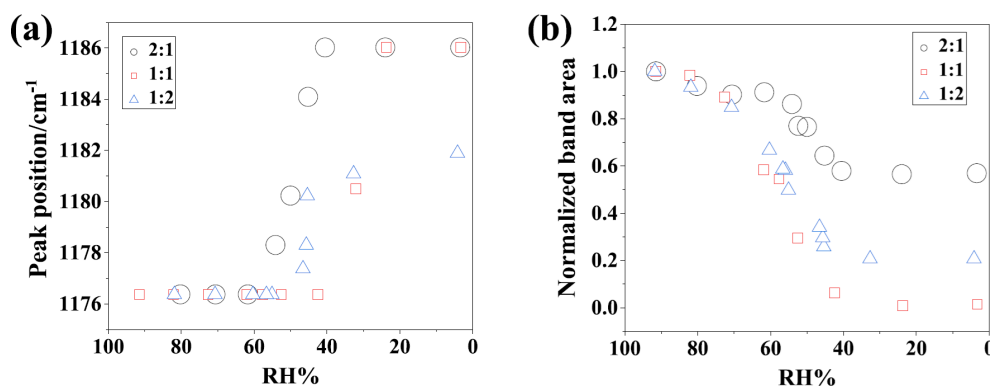
Figure 5. (a) The peak position shift from 1176 to 1186 cm^{-1} and **(b)** the integrated areas corresponding to integrated band areas for 2 : 1, 1 : 1, and 1 : 2 SP/NH$_4$Cl particles during the dehumidification.

particles. Thus, the onset of efflorescence relative humidity (ERH) can be identified by the appearance of the 1186 cm^{-1} peak. From Fig. 5a, the onsets of ERH were approximately 61.7 % and 23.7 % for 2 : 1 and 1 : 1 SP/NH$_4$Cl particles, respectively. However, for NH$_4$Cl-rich mixtures, the band at 1182 cm^{-1} rather than 1186 cm^{-1} was observed at the lowest RH of 4.2 %, indicating the formation of SP semi-solids due to the uptake of trace amounts of moisture. This suggests that the presence of NH$_4$Cl hindered the crystallization of SP.

The integrated absorbance spanning 1220 to 1120 cm^{-1} demonstrates the evolution of SP content during dehumidification in Fig. 5b. The data indicate values of approximately 0.56, 0.06, and 0.22 for 2 : 1, 1 : 1, and 1 : 2 SP/NH$_4$Cl mixtures, respectively, when the RH reached its minimum value. This implies that the degree of reaction was maximum when SP was mixed with NH$_4$Cl in equal moles, lending credence to the reaction mechanism proposed by Wang et al. (2019).

3.6 The impact of replacement reaction on the organic/ammonium sulfate aerosol phase state

The component evolution and aerosol phase transition are dependent upon multiple processes containing intermolecular interaction, ion mobility, gas–particle partitioning, ion-pair formation, replacement reaction, and dissociation, which originated from the composition of the internally mixed aerosols (Li et al., 2021; Mikhailov et al., 2004). In this section, various organic salts mixed with (NH$_4$)$_2$SO$_4$ were measured to explore the phase behaviors of atmospheric sulfate aerosols. Unlike SP, the applied sodium citrate (SC) and sodium tartrate (ST) exhibit a viscous state at lower RH without DRH and ERH.

Figure 6 displays the IR spectra of SC/(NH$_4$)$_2$SO$_4$ and ST/(NH$_4$)$_2$SO$_4$ particles on dehydration. In Fig. 6a, as the RH decreases, the bands at 1575 and 1391 cm^{-1} decreased, whereas the 1715 cm^{-1} peak gradually increased, which indicates a decrease in -COO$^-$ and an increase in -COOH. Other observations include the degenerated band at

1095 cm^{-1}. When the RH decreases to 56.9 %, the band at 1132 cm^{-1} appeared, as well as the band at 995 cm^{-1} for crystallized sulfate, indicating the crystalline solid Na$_2$SO$_4$ formation. As the RH further decreased, the 995 cm^{-1} band for crystalline sulfate became stronger, accompanying the weaker 980 cm^{-1} absorption peak, suggesting growing crystalline solid Na$_2$SO$_4$ content in the particles. For the ST/(NH$_4$)$_2$SO$_4$ mixture in Fig. 6b, we observed an increasing band at 1715 cm^{-1} and the replacement of the 1587 cm^{-1} band by the 1597 cm^{-1} band, indicating the transformation from sodium tartrate to sodium bitartrate. In addition, no crystalline solid formed in the aerosols since neither 1132 cm^{-1} nor 996 cm^{-1} was observed during the whole dehydration process.

Figure 7a shows the IR spectra as a function of RH for SC/(NH$_4$)$_2$SO$_4$ during the hydration process. As the RH increases, the band at 1132 cm^{-1} maintains a constant intensity below 70.5 % RH with a slight enhancement of water features. At 70.5 % RH, the band at 1132 cm^{-1} weakens with a notable increase in the 980 cm^{-1} band, indicating the onset of Na$_2$SO$_4$ dissolution. The aerosol, mainly consisting of Na$_2$SO$_4$, completely deliquesces at 87.2 % RH as the band at 996 cm^{-1} disappears entirely.

The IR spectra of ST/(NH$_4$)$_2$SO$_4$ particles are depicted in Fig. 7b. Upon hydration, bands at 1132 and 995 cm^{-1} are observed at 43.6 % RH, suggesting an unexpected formation of crystalline solid Na$_2$SO$_4$. As the RH further increases, the IR features of crystalline solid Na$_2$SO$_4$ weaken, almost disappearing at 84.6 % RH, indicating the deliquescence of Na$_2$SO$_4$. Similar unconventional behavior of "crystallization on hydration" was also observed for mixed gluconic acid–(NH$_4$)$_2$SO$_4$ and gluconic acid–NaCl aerosols using optical images, where crystalline solid (NH$_4$)$_2$SO$_4$ and NaCl formed upon hydration (Zhu et al., 2022). Likewise, optical images of ST/(NH$_4$)$_2$SO$_4$ were monitored to verify the phase and morphologies during an RH cycle. As shown in Fig. 8, the left-hand side images show the round and smooth particle on dehydration, indicative of a homogeneous aqueous state
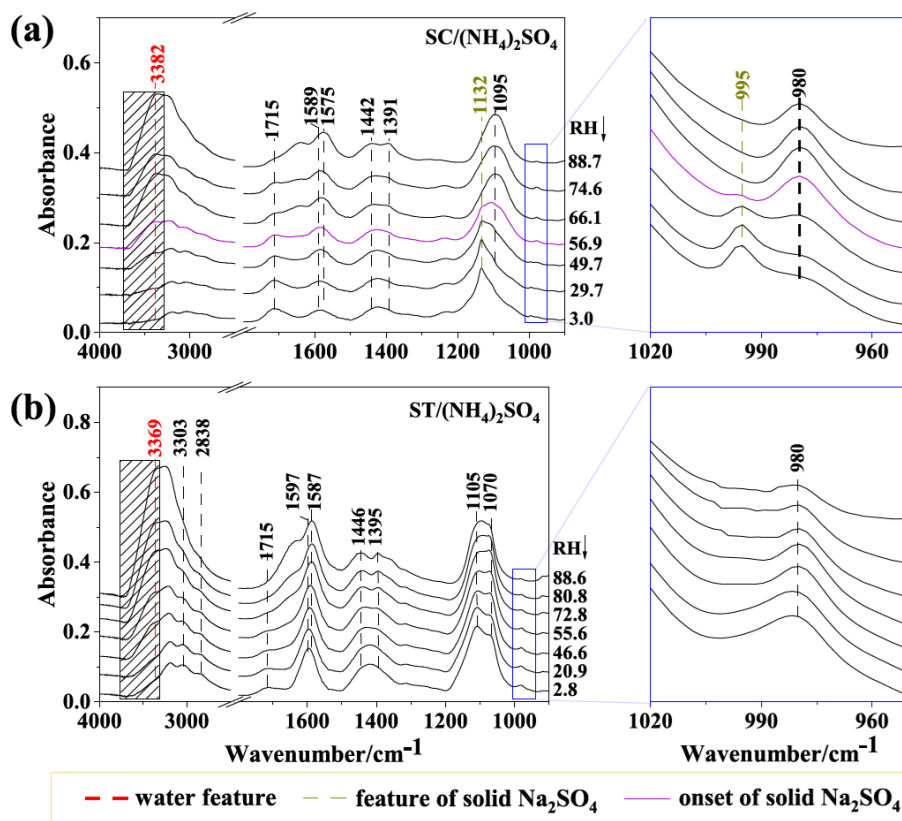
Figure 6. The FTIR spectra of **(a)** 2 : 3 SC/$(NH_4)_2SO_4$ and **(b)** 1 : 1 ST/$(NH_4)_2SO_4$ aerosols on dehydration.

without crystal formed until 12.1 %, which is consistent with the absence of the 996 cm^{-1} band in IR spectra (Fig. 6b). During humidification, the particles maintain a uniform state with a round shape below 44 % RH. At 44 % RH, some apparent rectangular dark entities, indicating crystalline solid formation, can be observed within the round particles. Combining the above IR features and morphologies, the aerosols at 44 % RH consist of crystalline solid Na_2SO_4, aqueous $(NH_4)_2SO_4$, and SC. When the RH increases to 80.3 % RH, the round and bright sphere is restored, indicating aerosol deliquescence.

As shown in Figs. 6 and 7, the IR spectra of SO_4^{2-} and organic salts remained distinguishable as the RH changes from ~ 88.7 % to ~ 2.0 % RH stepwise with a rate lower than 5 % RH min^{-1}, indicating incomplete reaction likely due to mass transfer limitations in viscous aerosol particles for about 30 min at every RH level. With higher viscosity, the degree of chemical reaction tends to decrease. Considering the correlation between the degree of replacement reaction and water content, if the reaction remains incomplete after an RH cycle, the water content in the solution state during hydration is lower than that during dehydration (X. Li et al., 2017). The gaps in water content between dehydration and hydration during two RH cycles are illustrated in Fig. S5 in the Supplement. For SP/$(NH_4)_2SO_4$ aerosols, full

recovery of water was observed after the second RH cycle, indicative of complete reaction and mainly Na_2SO_4 presence in the particles, which is consistent with the absence of IR absorptions from $(NH_4)_2SO_4$ and SP in Fig. S2a. However, for SC/$(NH_4)_2SO_4$ and ST/$(NH_4)_2SO_4$ mixed aerosols, the normal water absorption decreased by 0.1 and 0.14, respectively, after a second RH cycle, providing evidence of the viscous state of the mixed aerosols.

3.7 The Na_2SO_4 efflorescence upon hydration induced by the replacement reaction

Pöhlker et al. (2014) applied X-ray microspectroscopy to internally mixed aerosol particles from the Amazonian rainforest collected during anthropogenic pollution and found changes in particle microstructure upon hydration, primarily driven by efflorescence and recrystallization of sulfate salts during aerosol hydration. The efflorescence upon hydration was attributed to aerosol viscosity and surface tension. Upon hydration, the initially amorphous state of particles is in a metastable state where the formation of the crystalline solid phase is thermodynamically favored but kinetically hindered by nucleation. Continuous water uptake by the particles with rising RH is accompanied by decreasing aerosol viscosity and increasing ion mobility, which could overcome the kinetic inhibition of ion movement at a certain RH level, lead-
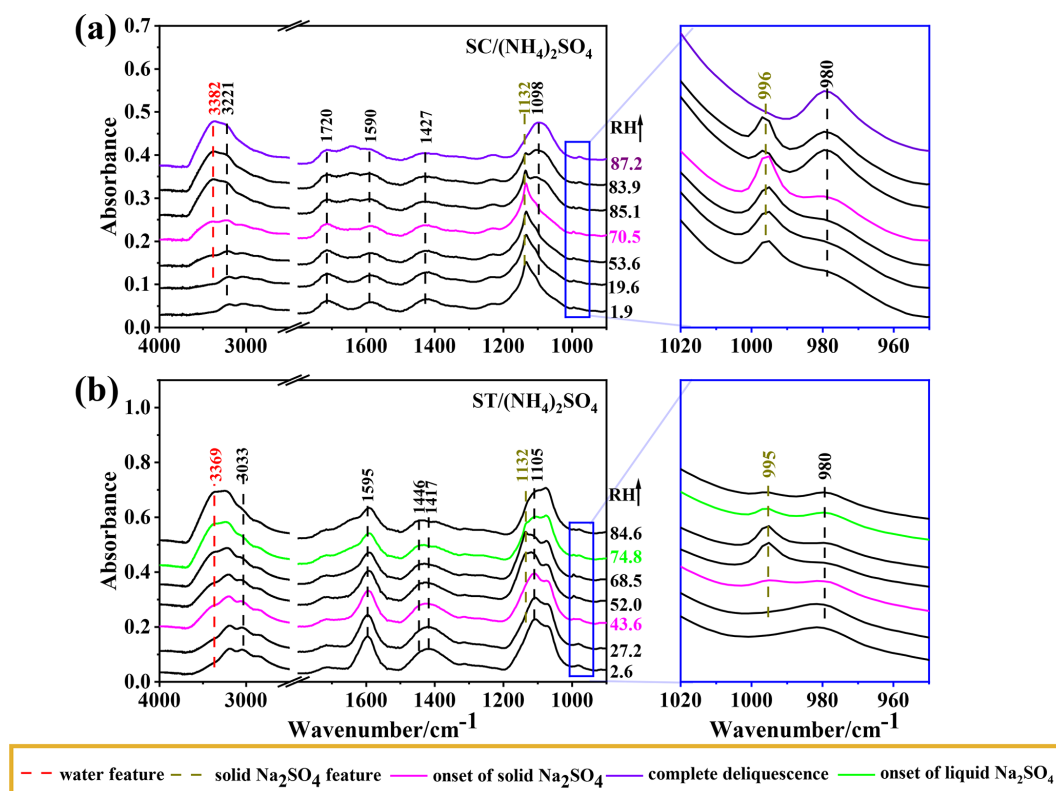
Figure 7. The FTIR spectra of **(a)** 2 : 3 SC/(NH$_4$)$_2$SO$_4$ and **(b)** 1 : 1 ST/(NH$_4$)$_2$SO$_4$ aerosols on hydration.
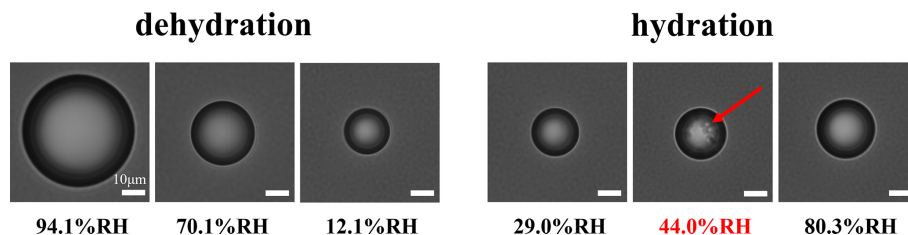

Figure 8. The optical morphologies of 1 : 1 ST/(NH$_4$)$_2$SO$_4$ aerosols during a down-up RH cycle. The red arrow points toward the location where the phase transition occurs. The RH indicated in red marks the occurrence of phase transitions. Scale bar represents 10μm.

ing to nucleation and crystal growth. However, the molecular structure was unknown in Pöhlker's study. Notwithstanding the viscous state for most organics, efflorescence upon hydration is rare. In fact, several previous studies on the phase state evolution of internally mixed organic/inorganic particles (Wang et al. 2019; Ma et al., 2022; Shao et al., 2018) have shown ordinary efflorescence upon dehydration, and to the best of our knowledge, no similar crystallization upon humidification has been reported besides Pöhlker's study. In this work, SC particles retained in a viscous state at lower RH levels as addressed above, while Na$_2$SO$_4$ crystallized upon dehydration from SC/(NH$_4$)$_2$SO$_4$ particles. Therefore, the effect of the molecular structure of organics on inorganic efflorescence needs to be further explored.

According to our recent study on mixed aerosols of gluconic acid and (NH$_4$)$_2$SO$_4$ or NaCl, and the Na$_2$SO$_4$ crystallization from ST and (NH$_4$)$_2$SO$_4$ mixtures observed herein, we found that polyhydroxy acids or organic salts containing full-hydroxyl carbon chains likely cause the efflorescence upon dehydration owing to more viscosity. Grayson et al. (2017) has defined increased viscosity as the number of hydroxyl groups in the molecule. As the RH decreases, the polyhydroxy chain with a carboxyl group is prone to form a gel owing to intermolecular hydrogen bonding. Gels are two-phase mixtures of liquids dispersed in (semi-)solid amorphous matrices, and the uptake of water into a gel can involve gradual swelling, as well as stepwise volume increases related to thermodynamically well-defined phase transitions (Pang and Zhu, 2002). When ST was mixed with
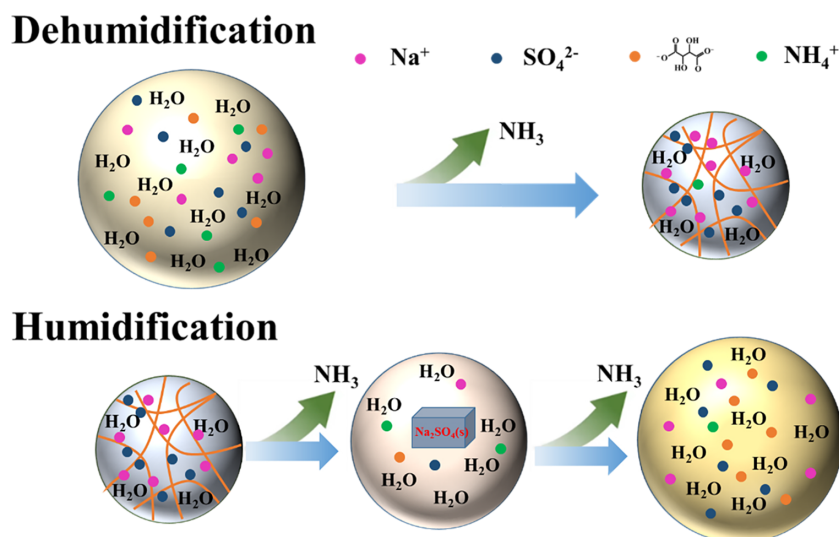
Figure 9. The schematic phase behavior and chemical process of 1 : 1 ST/$(NH_4)_2SO_4$ particles during dehumidification and humidification. The orange curve represents the fibrous gel.

$(NH_4)_2SO_4$, the polyhydroxy skeleton remained unchanged, and a gel structure gradually formed with the decrease in RH. Based on the gel state of internally mixed ST/$(NH_4)_2SO_4$ particles, the mechanism for efflorescence upon hydration was proposed (shown in Fig. 9). During the first RH cycle, the ions can transfer freely in the aqueous aerosol. As the RH decreased, tartrate ions and acidified hydrogen tartrate self-assembled into aggregates and gradually gelatinized water due to a decrease in water content, along with NH_3 release. Upon drying, gels can form highly porous structures (Li and Gong, 2024; Díaz-Marín et al., 2022). Therefore, in the gel structure, there may exist a collection of fine fibers in these gels where mechanical entanglements create a three-dimensional supramolecular structure to trap water molecules, owing to both the chemical adsorption of water molecules onto the gel fibers and the physical uptake of water due to capillary condensation (Fig. 9). Due to the strong interaction between OH groups and SO_4^{2-} ions, anions were bound around fibers. Hence, migration of SO_4^{2-} and Na^+ ions was inhibited so that these ions could not come into contact and nucleate a crystalline phase. The gel structure is a metastable state with a higher energy state than the crystalline state. Upon hydration following dehydration, the initial metastable aerosol can overcome the energy barrier to restore ion mobility in the particle; in turn, the anions and cations can combine to further form a solid nucleus, accompanying continuous NH_3 release. Continuously elevating RH provided more water content in particles, inducing crystal formation from the metastable state surrounded by a more stable solution employed gradually. Further water uptake can overcome the lattice energy to perform a crystalline solid-to-aqueous phase transition, resulting in complete dissolution of crystalline solid Na_2SO_4 and aerosol deliquescence.

4   Conclusions

Our findings illustrate that the aqueous replacement reaction within internally mixed organic/ammonium aerosols can alter the aerosol composition, which in turn affects the phase behavior of aerosol particles. The phase transition behaviors studied in this work are summarized in Table 2. As carboxylic acids and carboxylate salts are abundant in the internal mixtures of atmospheric secondary aerosols (Yang and Yu, 2008; Kawamura and Bikkina, 2016; Huang et al., 2022), our result implies that the aqueous-phase reactions are a significant process that can potentially dictate and complicate the phase behavior of internally mixed organic/inorganic aerosols. The change in ERH and DRH, as well as the occurrence of efflorescence upon humidification due to the replacement reaction in organic/ammonium aerosols, is crucial for the interaction between aerosols, water vapor, and trace gases and potentially causes uncertainty for the prediction of atmospheric aerosol phase states. Through the analysis of ATR-FTIR spectra from multiple organic/ammonium aerosol systems under RH cycling, we have provided valuable insights into the complex interactions between organic and inorganic components within aerosol particles.

By examining the hygroscopic behavior and phase transitions of internally mixed particles containing organic acid salts and ammonium salts, we have uncovered the occurrence of replacement reactions and aerosol component depletion during RH changes. Additionally, we observed unconventional crystallization upon hydration behavior for the organic/ammonium mixture aerosols, which can reduce the possibility of further composition evolution and reactive gas uptake due to the absence of ion mobility in the solid phase at higher RH. Hence, light absorbance and CCN ac-

Table 2. The phase transition behaviors of different organic salts and ammonium salts.

Mixed aerosols		SP mixed with					(NH$_4$)$_2$SO$_4$ mixed with	
		NH$_4$Cl			NH$_4$NO$_3$	(NH$_4$)$_2$SO$_4$	SC	ST
		2 : 1	1 : 1	1 : 2	(1 : 1)	(2 : 1)	3 : 2	1 : 1
ERH % on dehydration	SP NH$_4$Cl	61.7 ×	23.7 42.5	× 46.6	NaNO$_3$: 35.7–12.7 SP: ×	Na$_2$SO$_4$: 65.7–60.1 SP: ×	Na$_2$SO$_4$: 56.9 SC: ×	×
DRH % on hydration	SP NH$_4$Cl	84.3 ×	× 71.8	× 77.7	NaNO$_3$: 66.1–82.3 SP: ×	Na$_2$SO$_4$: 83.8–90.3 SP: ×	Na$_2$SO$_4$: 70.5–87.2 SC: ×	Na$_2$SO$_4$: 74.8
ERH % on hydration	×	×	×	×	×	×	×	Na$_2$SO$_4$: 43.6

Note: × means no phase transition was observed. The single value represents the onset of ERH or DRH.
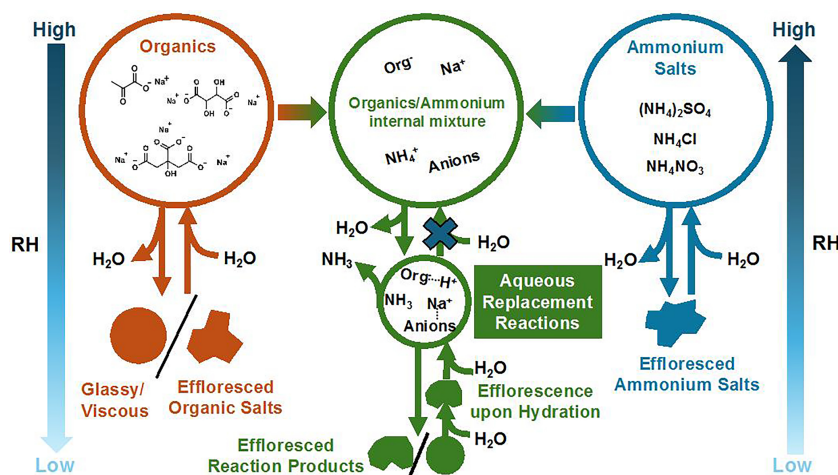
Figure 10. The schematic of the interplay between aqueous replacement reactions and the phase behavior of internally mixed organic/inorganic aerosols.

tivity, which strongly depend on chemical composition, will change. Future studies are needed to further investigate this phenomenon, as it is also expected to occur in other organic/inorganic aerosols that can potentially form into a gel-like state prior to typical efflorescence.

Our findings highlight the intricate interactions between chemical components of organic/inorganic aerosol (illustrated in Fig. 10). The interplay among the organic molecular structure, molar ratio, aqueous replacement reactions, and aerosol phase state can lead to unique and potentially irreversible aerosol evolution during RH cycles, for example, the special chemical process in aerosols induced by gel-state formation upon humidification. The observed variations in replacement reactions and product depletion, as well as phase transitions, emphasize the complexity of aqueous-phase aerosol chemistry and its impact on atmospheric processes.

Except for RH, aerosol phase also depends on other atmospheric conditions, particularly temperature. Solid ammonium sulfate particles with organic coatings were observed under high relative humidity (67 % to 98 %) at low temperatures (-2 to $+4$ °C), underscoring the key role of temperature in phase transitions (Kirpes et al., 2022). Kirpes et al. (2022) proposed that solid (NH$_4$)$_2$SO$_4$ formed through contact efflorescence and temperature-induced liquid–liquid phase separation (LLPS). Previous studies have shown that temperature often has a greater impact on LLPS than on efflorescence (Schill and Tolbert, 2013). LLPS is crucial for the solidification of ammonium sulfate (Roy et al., 2020) and soot redistribution (Yuan et al., 2023) in aqueous organic–inorganic aerosol droplets. In our work, we observed various aerosol phase states, including crystalline, aqueous, and gel-like states, during dehydration and hydration cycles, and we examined the interplay among aqueous-phase reactions, aerosol hygroscopicity, and phase behavior in detail. How-

ever, LLPS was not observed prior to crystallization, either through optical microscopy or ATR-FTIR. Future studies are needed to explore the interplay between various phase transitions, including LLPS, efflorescence, and viscous state formation, considering not only RH but also temperature. By understanding the diverse compositions and phase behaviors of internally mixed organic/inorganic aerosols, we can better address the challenges in air pollution remediation and climate change.

Author contributions. SP conceptualized and designed the study. YZ and SP supervised the study. HY, FD, and LX conducted the experiments. HY and SP analyzed and visualized the data and wrote the original draft. QH and SP reviewed and edited the paper.

References

Bouzidi, H., Zuend, A., Ondráèek, J., Schwarz, J., and Ždímal, V.: Hygroscopic behavior of inorganic–organic aerosol systems including ammonium sulfate, dicarboxylic acids, and oligomer, Atmos. Environ., 229, 117481, https://doi.org/10.1016/j.atmosenv.2020.117481, 2020.

Chen, Z., Liu, P., Liu, Y., and Zhang, Y.: Strong Acids or Bases Displaced by Weak Acids or Bases in Aerosols: Reactions Driven by the Continuous Partitioning of Volatile Products into the Gas Phase, Accounts Chem. Res., 54, 3667–3678, https://doi.org/10.1021/acs.accounts.1c00318, 2021.

Chen, Z., Liu, P., Su, H., and Zhang, Y.: Displacement of Strong Acids or Bases by Weak Acids or Bases in Aerosols: Thermodynamics and Kinetics, Environ. Sci. Technol., 56, 12937–12944, https://doi.org/10.1021/acs.est.2c03719, 2022.

Díaz-Marín, C. D., Zhang, L., Lu, Z., Alshrah, M., Grossman, J. C., and Wang, E. N.: Kinetics of Sorption in Hygroscopic Hydrogels, Nano Lett., 22, 1100–1107, https://doi.org/10.1021/acs.nanolett.1c04216, 2022.

Du, C., Yang, H., Wang, N., Pang, S., and Zhang, Y.: pH effect on the release of NH_3 from the internally mixed sodium succinate and ammonium sulfate aerosols, Atmos. Environ., 220, 11710, https://doi.org/10.1016/j.atmosenv.2019.117101, 2020.

Du, C., Wang, W., Wang, N., Pang, S., and Zhang, Y.: Impact of ambient relative humidity and acidity on chemical composition evolution for malonic acid/calcium nitrate mixed particles, Chemosphere, 276, 130140, https://doi.org/10.1016/j.chemosphere.2021.130140, 2021.

Freedman, M. A., Huang, Q., and Pitta, K. R.: Phase Transitions in Organic and Organic/Inorganic Aerosol Particles, Annu. Rev. Phys. Chem., 75, 257–281, https://doi.org/10.1146/annurev-physchem-083122-115909, 2024.

Grayson, J. W., Evoy, E., Song, M., Chu, Y., Maclean, A., Nguyen, A., Upshur, M. A., Ebrahimi, M., Chan, C. K., Geiger, F. M., Thomson, R. J., and Bertram, A. K.: The effect of hydroxyl functional groups and molar mass on the viscosity of non-crystalline organic and organic–water particles, Atmos. Chem. Phys., 17, 8509–8524, https://doi.org/10.5194/acp-17-8509-2017, 2017.

Herrmann, H., Schaefer, T., Tilgner, A., Styler, S. A., Weller, C., Teich, M., and Otto, T.: Tropospheric Aqueous-Phase Chemistry: Kinetics, Mechanisms, and Its Coupling to a Changing Gas Phase, Chem. Rev., 115, 4259–4334, https://doi.org/10.1021/cr500447k, 2015.

Hodas, N., Zuend, A., Mui, W., Flagan, R. C., and Seinfeld, J. H.: Influence of particle-phase state on the hygroscopic behavior of mixed organic–inorganic aerosols, Atmos. Chem. Phys., 15, 5027–5045, https://doi.org/10.5194/acp-15-5027-2015, 2015.

Huang, R.-J., Zhang, Y., Bozzetti1, C., Ho, K.-F., Cao, J.-J., Han, Y., Daellenbach, K. R., Slowik, J. G., Platt, S. M., Canonaco, F., Zotter, P., Wolf, R., Pieber, S. M., Bruns, E. A., Crippa, M., Ciarelli, G., Piazzalunga, A., Schwikowski, M., Abbaszade, G., Schnelle-Kreis, J., Zimmermann, R., An, Z., Szidat, S., Baltensperger, U., Haddad, I. E., and Prévôt, A. S. H.: High secondary aerosol contribution to particulate pollution during haze events in China, Nature, 514, 218–222, https://doi.org/10.1038/nature13774, 2014.

Huang, S., Wu, Z., Wang, Y., Poulain, L., Höpner, F., Merkel, M., Herrmann, H., and Wiedensohler, A.: Aerosol Hygroscopicity and its Link to Chemical Composition in

a Remote Marine Environment Based on Three Transatlantic Measurements, Environ. Sci. Technol., 56, 9613–9622, https://doi.org/10.1021/acs.est.2c00785, 2022.

Jing, B., Tong, S., Liu, Q., Li, K., Wang, W., Zhang, Y., and Ge, M.: Hygroscopic behavior of multicomponent organic aerosols and their internal mixtures with ammonium sulfate, Atmos. Chem. Phys., 16, 4101–4118, https://doi.org/10.5194/acp-16-4101-2016, 2016.

Kawamura, K. and Bikkina, S.: A review of dicarboxylic acids and related compounds in atmospheric aerosols: Molecular distributions, sources and transformation, Atmos. Res., 170, 140–160, https://doi.org/10.1016/j.atmosres.2015.11.018, 2016.

Kirpes, R. M., Lei, Z., Fraund, M., Gunsch, M. J., May, N. W., Barrett, T. E., Moffett, C. E., Schauer, A. J., Alexander, B., Upchurch, L. M., China, S., Quinn, P. K., Moffet, R. C., Laskin, A., Sheesley, R. J., Pratt., K. A., and Ault, A. P.: Solid organic-coated ammonium sulfate particles at high relative humidity in the summertime Arctic atmosphere, P. Natl. Acad. Sci. USA, 119, e2104496119, https://doi.org/10.1073/pnas.2104496119, 2022.

Kreidenweis, S. M., Koehler, K., DeMott, P. J., Prenni, A. J., Carrico, C., and Ervens, B.: Water activity and activation diameters from hygroscopicity data – Part I: Theory and application to inorganic salts, Atmos. Chem. Phys., 5, 1357–1370, https://doi.org/10.5194/acp-5-1357-2005, 2005.

Kuang, Y., Xu, W., Tao, J., Ma, N., Zhao C., and Shao, M.: A Review on Laboratory Studies and Field Measurements of Atmospheric Organic Aerosol Hygroscopicity and Its Parameterization Based on Oxidation Levels, Curr. Poll. Rep., 6, 410–424, https://doi.org/10.1007/s40726-020-00164-2, 2010.

Li, Q., Ma. S., Liu, Y., Wu, X., Fu, H., Tu, X., Yan, S., Zhang, L., George, C., and Chen, J.: Phase State Regulates Photochemical HONO Production from NaNO$_3$/Dicarboxylic Acid Mixtures, Environ. Sci. Technol., 58, 7516–7528, https://doi.org/10.1021/acs.est.3c10980, 2024.

Li, W., Teng, X., Chen, X., Liu, L., Xu, L., Zhang, J., Wang, Y., Zhang, Y., and Shi Z.: Organic Coating Reduces Hygroscopic Growth of Phase-Separated Aerosol Particles, Environ. Sci. Technol., 55, 16339–16346, https://doi.org/10.1021/acs.est.1c05901, 2021.

Li, X. and Gong, J. P.: Design principles for strong and tough hydrogels, Nat. Rev. Mater., 9, 380–398, https://doi.org/10.1038/s41578-024-00672-3, 2024.

Li, X., Gupta, D., Lee, J., Park, G., and Ro, C. U.: Real-time investigation of chemical compositions and hygroscopic properties of aerosols generated from NaCl and malonic acid mixture solutions using in situ Raman microspectrometry, Environ. Sci. Technol., 51, 263–270, https://doi.org/10.1021/acs.est.6b04356, 2017.

Li, Y.-J., Liu, P.-F., Bergoend, C., Bateman A. P., and Martin, S. T.: Rebounding hygroscopic inorganic aerosol particles: Liquids, gels, and hydrates, Aerosol Sci. Tech., 51, 388–396, https://doi.org/10.1080/02786826.2016.1263384, 2017.

Liu, P., Li, Y. J., Wang, Y., Gilles, M. K., Zaveri, R. A., Bertram, A. K., and Martin, S. T.: Lability of Secondary Organic Particulate Matter, P. Natl. Acad. Sci. USA, 113, 12643–12648, https://doi.org/10.1073/pnas.1603138113, 2016.

Ma, Q., Zhong, C., Liu, C., Liu, J., Ma, J., Wu, L., and He, H.: A Comprehensive Study about the Hygroscopic Behavior of Mixtures of Oxalic Acid and Nitrate Salts: Im-

plication for the Occurrence of Atmospheric Metal Oxalate Complex, ACS Earth Space Chem., 3, 1216–1225, https://doi.org/10.1021/acsearthspacechem.9b00077, 2019.

Ma, S., Li, Q., and Zhang, Y.: A comprehensive study on hygroscopic behaviour and nitrate depletion of NaNO$_3$ and dicarboxylic acid mixtures: implications for nitrate depletion in tropospheric aerosols, Atmos. Chem. Phys., 22, 10955–10970, https://doi.org/10.5194/acp-22-10955-2022, 2022.

Madawala, C. K., Lee, H. D., Kaluarachchi, C. P., and Tivanski, A. V.: Probing the Water Uptake and Phase State of Individual Sucrose Nanoparticles Using Atomic Force Microscopy, ACS Earth Space Chem., 5, 2612–2620, https://doi.org/10.1021/acsearthspacechem.1c00101, 2021.

Marcolli, C. and Krieger, U. K.: Phase Changes during Hygroscopic Cycles of Mixed Organic/Inorganic Model Systems of Tropospheric Aerosols, J. Phys. Chem. A, 110, 1881–1893, https://doi.org/10.1021/jp0556759, 2006.

Martin, S. T.: Phase Transitions of Aqueous Atmospheric Particles, Chem. Rev., 100, 3403–3453, https://doi.org/10.1021/cr990034t, 2000.

Max, J.-J. and Chapados, C.: Aqueous ammonia and ammonium chloride hydrates: principal infrared spectra, J. Mol. Struct., 1046, 124–135, https://doi.org/10.1016/j.molstruc.2013.04.045, 2013.

Mikhailov, E., Vlasenko, S., Niessner, R., and Pöschl, U.: Interaction of aerosol particles composed of protein and saltswith water vapor: hygroscopic growth and microstructural rearrangement, Atmos. Chem. Phys., 4, 323–350, https://doi.org/10.5194/acp-4-323-2004, 2004.

Mikhailov, E., Vlasenko, S., Martin, S. T., Koop, T., and Pöschl, U.: Amorphous and crystalline aerosol particles interacting with water vapor: conceptual framework and experimental evidence for restructuring, phase transitions and kinetic limitations, Atmos. Chem. Phys., 9, 9491–9522, https://doi.org/10.5194/acp-9-9491-2009, 2009.

Miñambres, L., Méndez, E., Sánchez, M. N., Castaño, F., and Basterretxea, F. J.: Water uptake of internally mixed ammonium sulfate and dicarboxylic acid particles probed by infrared spectroscopy, Atmos. Environ., 70, 108–116, https://doi.org/10.1016/j.atmosenv.2013.01.007, 2013.

Nemesure, S., Wagener, R., and Schwartz, S. E.: Direct Shortwave Forcing of Climate by the Anthropogenic Sulfate Aerosol: Sensitivity to Particle Size, Composition, and Relative Humidity, J. Geophys. Res., 100, 26105–26116, https://doi.org/10.1029/95JD02897, 1995.

Pang, S. and Zhu, D.: Pronounced hydrogel formation by the self-assembled aggregate of semifluorinated fatty acid, Chem. Phys. Lett., 358, 479–483, https://doi.org/10.1016/S0009-2614(02)00646-2, 2002.

Petters, M. D. and Kreidenweis, S. M.: A single parameter representation of hygroscopic growth and cloud condensation nucleus activity, Atmos. Chem. Phys., 7, 1961–1971, https://doi.org/10.5194/acp-7-1961-2007, 2007.

Pöhlker, C., Saturno, J., Krüger, M. L., Förster, J.-D., Weigand, M., Wiedemann, K. T., Bechtel, M., Artaxo, P., and Andreae, M. O.: Efflorescence upon humidification? X-ray microspectroscopic in situ observation of changes in aerosol microstructure and phase state upon hydration, Geophys. Res. Lett., 41, 3681–3689, https://doi.org/10.1002/2014GL059409, 2014.

Reid, J. P., Bertram, A. K., Topping, D. O., Laskin, A., Martin, S. T., Petters, M. D., Pope, F. D., and Rovelli, G.: The viscosity of atmospherically relevant organic particles, Nat. Commun., 9, 956, https://doi.org/10.1038/s41467-018-03027-z, 2018.

Ren, H., Cai, C., Leng, C.-B., Pang, S.-F., and Zhang, Y.-H.: Nucleation Kinetics in Mixed $NaNO_3$/Glycerol Droplets Investigated with the FTIR–ATR Technique, J. Phys. Chem. B, 120, 2913–2920, https://doi.org/10.1021/acs.jpcb.5b12442, 2016.

Riemer, N., Ault, A. P., West, M., Craig, R. L., and Curtis, J. H.: Aerosol Mixing State: Measurements, Modeling, and Impacts, Rev. Geophys., 57, 187–249, https://doi.org/10.1029/2018RG000615, 2019.

Roy, P., Mael, L. E., Makhnenko, I., Martz, R., Grassian, V. H., and Dutcher, C. S.: Temperature-Dependent Phase Transitions of Aqueous Aerosol Droplet Systems in Microfluidic Traps, ACS Earth Space Chem., 4, 1527–1539, https://doi.org/10.1021/acsearthspacechem.0c00114, 2020.

Shao, X., Wu, F.-M., Yang, H., Pang, S.-F., and Zhang, Y.-H.: Observing HNO_3 release dependent upon metal complexes in malonic acid/nitrate droplets, Spectrochim. Acta A, 201, 399–404, https://doi.org/10.1016/j.saa.2018.05.026, 2018.

Schill, G. P. and Tolbert, M. A.: Heterogeneous ice nucleation on phase-separated organic-sulfate particles: effect of liquid vs. glassy coatings, Atmos. Chem. Phys., 13, 4681–4695, https://doi.org/10.5194/acp-13-4681-2013, 2013.

Schroeder, J. R. and Beyer, K. D.: Deliquescence relative humidities of organic and inorganic salts important in the atmosphere, J. Phys. Chem. A, 120, 9948–9957, https://doi.org/10.1021/acs.jpca.6b08725, 2016.

Shi, X. M., Wu, F. M., Jing, B., Wang, N., Xu, L. L., Pang, S. F., and Zhang, Y. H.: Hygroscopicity of internally mixed particles composed of $(NH_4)_2SO_4$ and citric acid under pulsed RH change, Chemosphere, 188, 532–540, https://doi.org/10.1016/j.chemosphere.2017.09.024, 2017.

Shiraiwa, M., Pfrang, C., Koop, T., and Pöschl, U.: Kinetic multilayer model of gas-particle interactions in aerosols and clouds (KM-GAP): linking condensation, evaporation and chemical reactions of organics, oxidants and water, Atmos. Chem. Phys., 12, 2777–2794, https://doi.org/10.5194/acp-12-2777-2012, 2012.

Tan, D.-T., Cai, C., Zhang, Y., Wang, N., Pang, S.-F., and Zhang, Y.-H.: Crystallization kinetics from mixture Na_2SO_4/glycerol droplets of Na_2SO_4 by FTIR-ATR, Chem. Phys., 485, 131–135, https://doi.org/10.1016/j.chemphys.2016.07.007, 2014.

Trebs, I., Metzger, S., Meixner, F. X., Helas, G. N., Hoffer, A., Rudich, Y., Falkovich, A. H., Moura, M. A. L., da Silva, R. S., Artaxo, P., Slanina, J., and Andreae, M. O.: The NH^{4+}-NO_3^--Cl^--SO_4^{2-}-H_2O aerosol system and its gas phase precursors at a pasture site in the amazon basin: How relevant are mineral cations and soluble organic acids?, J. Geophys. Res.-Atmos., 110, D07303, https://doi.org/10.1029/2004JD005478, 2005.

Wang, N., Cai, C., He, X., Pang, S.-F., and Zhang, Y.-H.: Vacuum FTIR study on the hygroscopicity of magnesium acetate aerosols, Spectrochim. Acta A, 192, 420–426, https://doi.org/10.1016/j.saa.2017.11.058, 2018.

Wang, N., Jing, B., Wang, P., Wang, Z., Li, J., Pang, S., Zhang, Y., and Ge, M.: Hygroscopicity and Compositional Evolution of Atmospheric Aerosols Containing Water-Soluble Carboxylic Acid Salts and Ammonium Sulfate: Influence of Am-

monium Depletion, Environ. Sci. Technol., 53, 6225–6234, https://doi.org/10.1021/acs.est.8b07052, 2019.

Wang, X., Jing, B., Tan, F., Ma, J., Zhang, Y., and Ge, M.: Hygroscopic behavior and chemical composition evolution of internally mixed aerosols composed of oxalic acid and ammonium sulfate, Atmos. Chem. Phys., 17, 12797–12812, https://doi.org/10.5194/acp-17-12797-2017, 2017.

Wu, Z. J., Nowak, A., Poulain, L., Herrmann, H., and Wiedensohler, A.: Hygroscopic behavior of atmospherically relevant water-soluble carboxylic salts and their influence on the water uptake of ammonium sulfate, Atmos. Chem. Phys., 11, 12617–12626, https://doi.org/10.5194/acp-11-12617-2011, 2011.

Yang, H., Wang, N., Pang, S., Zheng, C., and Zhang, Y.: Chemical reaction between sodium pyruvate and ammonium sulfate in aerosol particles and resultant sodium sulfate efflorescence, Chemosphere, 215, 554–562, https://doi.org/10.1016/j.chemosphere.2018.10.062, 2019.

Yang, L. and Yu, L. E.: Measurements of Oxalic Acid, Oxalates, Malonic Acid, and Malonates in Atmospheric Particulates, Environ. Sci. Technol., 42, 9268–9275, https://doi.org/10.1021/es801820z, 2008.

Yeung, M. C. and Chan, C. K.: Water Content and Phase Transitions in Particles of Inorganic and Organic Species and their Mixtures Using Micro-Raman Spectroscopy, Aerosol Sci. Tech., 44, 269–280, https://doi.org/10.1080/02786820903583786, 2010.

Yuan, Q., Wang, Y., Chen, Y., Yue, S., Zhang, J., Zhang, Y., Xu, L., Hu, W., Liu, D., Fu, P., Gao, H., and Li, W.: Measurement report: New insights into the mixing structures of black carbon on the eastern Tibetan Plateau – soot redistribution and fractal dimension enhancement by liquid–liquid phase separation, Atmos. Chem. Phys., 23, 9385–9399, https://doi.org/10.5194/acp-23-9385-2023, 2023.

Zhang, J., Wang, Y., Teng, X., Liu, L., Xu, Y., Ren, L., Shi, Z., Zhang, Y., Jiang, J., Liu, D., Hu, M., Shao, L., Chen, J., Martin, S. T., Zhang, X., and Li, W.: Liquid–liquid phase separation reduces radiative absorption by aged black carbon aerosols, Comm. Earth Environ., 3, 128, https://doi.org/10.1038/s43247-022-00462-1, 2022.

Zhang, Q. N., Zhang, Y., Cai, C., Guo, Y. C., Reid, J. P., and Zhang, Y. H.: In situ observation on the dynamic process of evaporation and crystallization of sodium nitrate droplets on a ZnSe substrate by FTIR-ATR, J. Phys. Chem. A, 118, 2728–37, https://doi.org/10.1021/jp412073c, 2014.

Zhang, Z., Li, Y., Ran, H., An, J., Qu, Y., Zhou, W., Xu, W., Hu, W., Xie, H., Wang, Z., Sun, Y., and Shiraiwa, M.: Simulated phase state and viscosity of secondary organic aerosols over China, Atmos. Chem. Phys., 24, 4809–4826, https://doi.org/10.5194/acp-24-4809-2024, 2024.

Zhou, S., Hwang, B. C. H., Lakey, P. S. J., Zuend, A., Abbatt, J. P. D., and Shiraiwa, M.: Multiphase reactivity of polycyclic aromatic hydrocarbons is driven by phase separation and diffusion limitations, P. Natl. Acad. Sci. USA, 116, 11658–11663, https://doi.org/10.1073/pnas.1902517116, 2019.

Zhu, Y., Pang, S., and Zhang, Y.: Observations on the unique phase transitions of inorganics relevant due to gluconic acid in particles, Atmos. Environ., 288, 119313, https://doi.org/10.1016/j.atmosenv.2022.119313, 2022.

Zong, T., Wang, H., Wu, Z., Lu, K., Wang, Y., Zhu, Y., Shang, D., Fang, X., Huang, X., He, L., Ma, N., Größ, J., Huang,

S., Guo, S., Zeng, L., Herrmann, H., Wiedensohler, A., Zhang, Y., and Hu, M.: Particle hygroscopicity inhomogeneity and its impact on reactive uptake, Sci. Total Environ., 811, 151364, https://doi.org/10.1016/j.scitotenv.2021.151364, 2022.